Deformation of a nanoporous silica under compressive loading

Aijie Han, Venkata K. Punyamurthula, Weiyi Lu, and Yu Qiao[a)]
Department of Structural Engineering, University of California—San Diego, La Jolla, California 92093-0085, USA

(Received 19 December 2007; accepted 25 February 2008; published online 30 April 2008)

In a compression experiment on a nanoporous silica gel, it is observed that at a high pressure the collapse of nanoporous structure provides a mechanism for plastic deformation, leading to an energy absorption efficiency much higher than that of many conventional protection and damping materials. Even though the network material is brittle, the overall behavior of the silica gel is ductile. After the compression test, the nanopore volume is largely reduced while the variation in nanopore surface area is secondary. According to a first-order poromechanic analysis, the effective plastic deformation is dominated by the buckling of the nanopore walls parallel to the external loading.
 [DOI: 10.1063/1.2909976]

I. INTRODUCTION

Cellular materials, such as honeycombs and metallic/polymer foams, are widely applied in energy absorption structures.[1,2] Common examples include expanded polypropylene and polystyrene in helmets and packaging systems, composite sandwich panels in vehicle bumpers, aluminum foams in blast-resistant containers, etc.[3–5] These materials contain large volume fractions of cells, and therefore are lightweight and of superior thermal insulation properties. More importantly, when subjected to compressive loadings the cell walls can buckle,[6] which absorbs a large amount of mechanical energy, attractive for damping and protection applications. The cells are usually produced by using foaming reagents and/or bubble generators prior to solidification.[7] Depending on the porosity, the cell size, as well as the mixing/solidification techniques, the cells can be either closed or open.[8] The cell size is typically 0.1–10 mm.[9] Cells smaller or larger than this range can be unstable.[10]

One intrinsic difficulty in developing higher-performance cellular materials is related to the relatively long characteristic time of cell-wall buckling. As an order-of-magnitude approximation, the buckling time, t_b, may be taken as $1/\omega$, where ω is the resonance frequency of the cell wall. For a cantilever-beam-type structure, $t_b=\alpha^*\sqrt{\rho/EI}\cdot d^2$,[11] where d is the cell size, ρ is the weight density, EI is the bending stiffness, and α^* is a geometry factor around 0.1–0.3. For most of the engineering cellular materials, t_b is in the range of a few milliseconds to a fraction of second, longer than the traveling time of a stress wave across the cell. Therefore, while cell-wall buckling can significantly lower the peak pressure, the profile of the wave front is often not affected. In order to solve this problem, t_b must be decreased to the μs or sub-μs level, for which the cell size, d, needs to be reduced by a few orders of magnitude to the nm scale. This concept can also be regarded as the promotion of high-order buckling modes. If the cell wall size is large, the first-order mode is most energetically favorable.[12] Recent research has shown that if soft joints are installed, they would trigger higher-order buckling modes under a relatively low pressure, and thus both temporal and spatial characteristics of buckling patterns are adjusted.[13] Decreasing the cell size can be of a similar effect. As a large cell breaks down into a number of smaller ones, the motion of cell walls parallel to the external loading would be constrained by the cell walls normal to the loading, and thus low-order buckling modes cannot take place.

When the cell size is 1–50 nm, the material becomes nanoporous. The synthesis procedure of a nanoporous material is very different from that of ordinary cellular materials. Usually, molecular templates are used.[14] Through thermal and/or chemical treatment, the template precipitates out of the network, and after it is removed via combustion or extraction, empty space is left in the network as nanopores.[15] The nanopore volume fraction is typically 10%–80%, and the specific surface area is 100–200 m^2/g. Over the years, a number of studies have been carried out on mechanical properties of nanoporous materials.[16–18] Most of them were focused on ductile materials, such as copper and gold. For brittle materials, such as silica or silicate, previous research was mainly for fracture in thin films.[19,20] Investigation on their behaviors under compression loadings is still scarce.

Recently, novel protection and damping systems were developed by using nanoporous silica particles suspended in liquids.[21–25] The nanopore surfaces were usually modified so that they were nonwettable. As the external loading reached a critical value, pressure induced infiltration could occur. Due to the ultralarge nanopore surface area and the high degree of hysteresis of sorption curves, the systems were energy absorbing. The nanoporous material functionalized (NMF) liquids can be utilized to fill the cells in a regular cellular material so as to enhance its performance.[26] In such a system, it was observed that in addition to the infiltration of pressurized liquid, the eventual collapse of nanoporous structure also provided a beneficial energy-absorption mechanism.

[a)]Author to whom correspondence should be addressed. Electronic mail: yqiao@ucsd.edu.

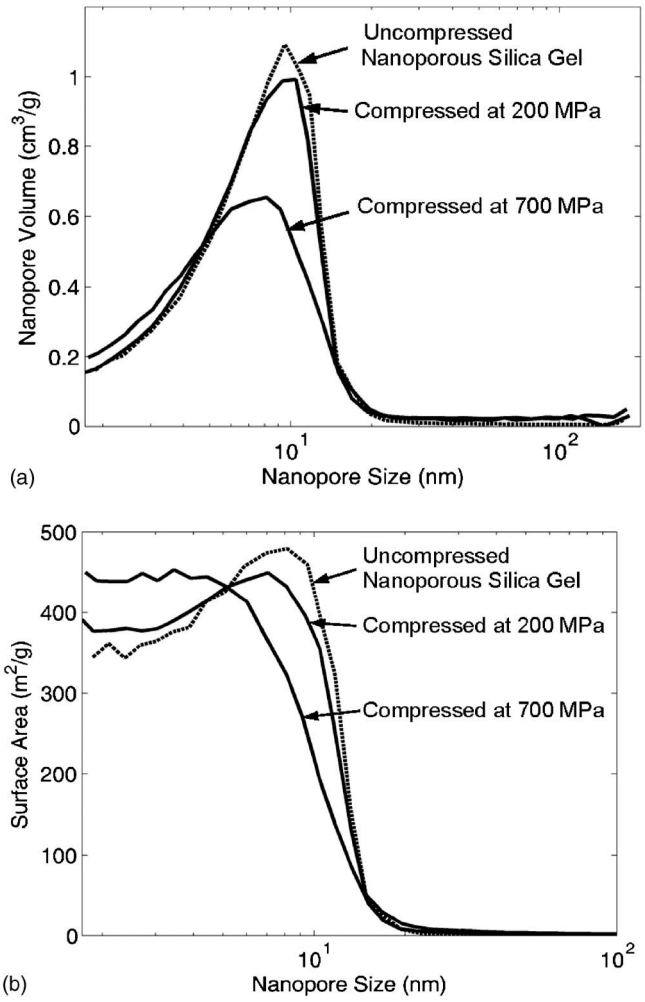

FIG. 1. Gas absorption analysis results of the nanoporous silica gel sample: (a) the nanopore volume distributions and (b) the nanopore surface area distribution.

II. EXPERIMENTAL

In order to investigate nanoporous silica behaviors, a silica hydrosol was first produced by refluxing water glass that contained 5.6% Na_2O and 14.9% SiO_2 and 3M sulphuric acid solution. Silica hydrosol was extracted by a needle valve. The reactor was kept in a water bath at room temperature. The *p*H value was maintained at 3.5, so that the specific micropore volume was minimized.[27] The hydrosol was washed in distilled water repeatedly, and set for 24 h, leading to the formation of nanoporous silica gel. The gel particles were then dried in a continuous air flow at 100 °C for 3 h. Their nanoporous structure was characterized by using a Micromeritics TriStar-3000 gas absorption analyzer, and the results of nanopore volume and nanopore surface area distributions are shown in Figs. 1(a) and 1(b), respectively.

The synthesized nanoporous silica gel particles were placed in an air-hardened steel cylinder and compressed by a steel piston. By using a type 5569 Instron machine, the piston was intruded into the cylinder at a constant rate of 1 mm/min. At the first loading, when the pressure reached 200 MPa, the piston was moved out at the same rate. The same loading-unloading process was repeated, after which the loosely packed particles were consolidated into a disk. Then,

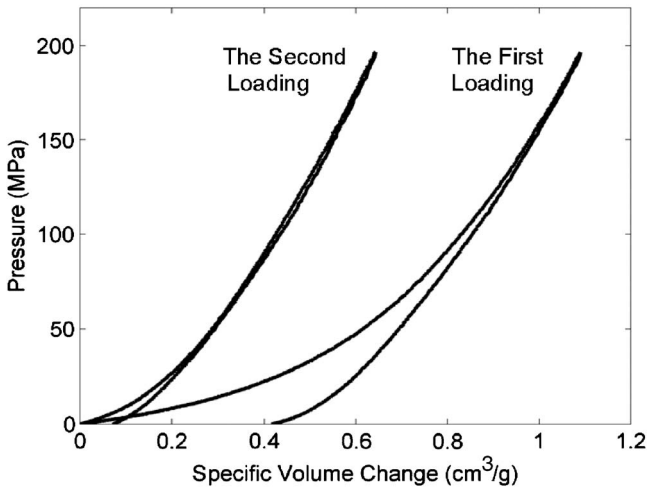

FIG. 2. Typical load-displacement curves of a low-pressure test. The curves have been shifted horizontally.

with the same loading rate, the nanoporous silica disk was compressed to 750 MPa for two cycles. Figures 2 and 3 show typical load-displacement curves. After each loading, about 0.1 g of silica gel was harvested for gas-absorption analysis, following which the samples were dissolved in methanol and dried by vacuum filtering, and then their weight densities were measured. The data of nanoporous structures are listed in Table I. The dried sample was also observed in an environmental electron scanning microscope (SEM). Figure 4 shows typical micrographs.

III. RESULTS AND DISCUSSION

The results of the porosity analysis in Fig. 1 indicate clearly that the synthesized silica gel is mesoporous. The nanopore volume distribution curve has the modal value of 9.4 nm. The most probable nanopore size in the surface area distribution curve is slightly smaller, around 8.3 nm, since larger nanopores have smaller specific surface areas. Most of the pore volume is associated with the nanopores of sizes in the range of 5–15 nm; the contribution of nanopores smaller

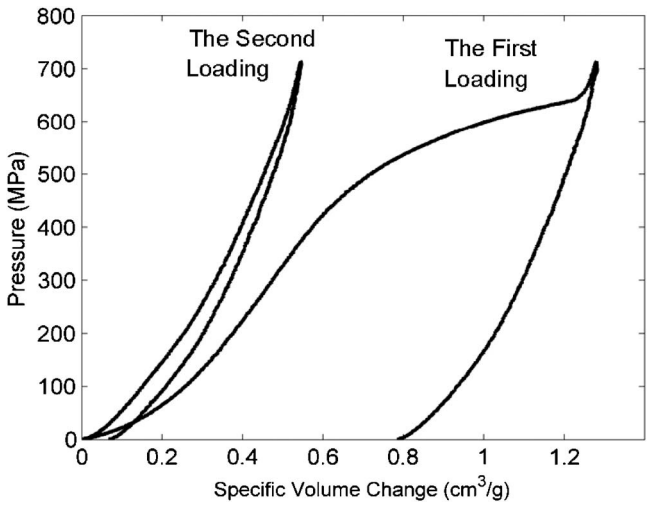

FIG. 3. Typical load-displacement curves of a high-pressure test. The curves have been shifted horizontally.

TABLE I. The nanoporous structures of the silica samples before and after the compression tests.

	Average nanopore radius (nm)	Specific nanopore surface area (m^2/g)	Specific nanopore volume (cm^3/g)	Weight density (mg/cm^3)
Before compression test	5.4	272	0.54	742
After being compressed at 200 MPa	5.3	272	0.53	761
After being compressed at 750 MPa	4.7	267	0.34	1128

than 3 nm or larger than 18 nm is negligible. However, the surface area of the smallest nanopores is only slightly smaller than the peak value.

In the low-pressure compression test, as shown in Fig. 2, no clear pressure plateau can be observed. With the increasing of compression volume, the pressure increases gradually to the set point of 200 MPa. As the load is reduced, while initially the unloading path and the loading path overlap with each other, the linearity of the unloading curve is maintained quite well even in the low-pressure range, until the external load entirely vanishes. Thus, there is a significant residual deformation, primarily due to the close-packing of the silica particles. The changes in nanopore surface area distribution and nanopore volume distribution are quite small (Fig. 1), suggesting that the nanopores remain stable. This is confirmed by the SEM observation that before [Fig. 4(a)] and after [Fig. 4(b)] the low-pressure compression experiment the frameworks of silica particles are similar. The relative probability of nanopore size distribution at the peak value decreases by about 8%, and that of the smallest nanopores slightly increases, i.e., a small portion of large nanopores are broken down into smaller ones, probably related to the collapse and fracture of the nanopores close to particle surfaces. The change in porous structure in the largest nanopore size range is not detectable. There are no considerable variations in the average nanopore size, the total nanopore surface area, the total nanopore volume, as well as the weight density.

As the second loading cycle is applied, the compressibility of the particle cluster becomes much smaller. Compared with the first loading path, the pressure reaches the peak value with a much smaller displacement. The slope of the compression curve is close to that of the final linear stage of the first loading. The unloading path is nearly identical with the loading path, and both of them are about the same as the first unloading path, that is, the packing of silica partciles has been saturated.

When the nanoporous silica disk is compressed at a higher pressure, as shown in Fig. 3, the testing curve exhibits entirely different characteristics. As the pressure is relatively low, the loading path resembles that of the low-pressure test. When the pressure exceeds about 400 MPa, the slope considerably decreases, indicating that the system compressibility increases. In the pressure range of 400–650 MPa, a plateau is formed. The width of the plateau is about 0.5 cm^3/g, quite close to the specific nanopore volume. SEM microscopy [Fig. 4(c)] indicates that the silica particles are crushed and fractured. When the pressure is higher than this range, the system compressibility rapidly decreases. Upon unloading, the pressure-displacement curve is relatively linear, except for the final low-pressure section. The slope of the high-pressure section of the unloading path is similar to the slope of the final stage of the loading path. The high degree of hysteresis causes a large residual deformation. As the high-pressure loading-unloading cycle is repeated, the system behavior becomes quite linear. No compression plateau can be

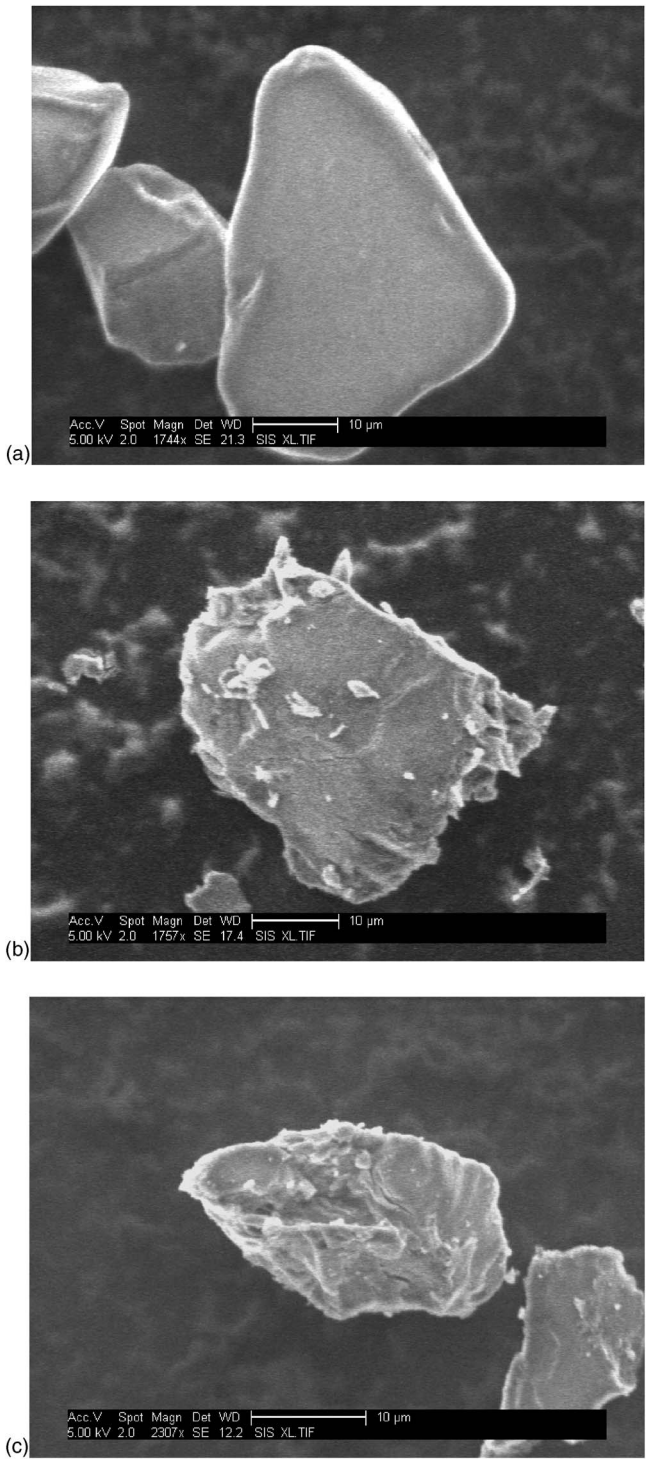

FIG. 4. Typical SEM microscopy of silica particles (a) before the compression test, (b) after the low-pressure compression test, and (c) after the high-pressure compression test.

observed. Both the loading and the unloading paths are of similar slopes to that of the unloading path of the first cycle.

According to the TriStar-3000 analysis, after the high-pressure compression, the nanopore volume distribution changes considerably. Clearly, the compression plateau in Fig. 3 is associated with the collapse of nanopores. The maximum volume decreases by nearly 50%, and the peak becomes flatter, i.e., the nanopore volume distributes over a broader range of nanopore size. The volume of relatively small nanopores increases, which suggests that larger nanopores are "shrunk" or broken down into smaller nanopores. The changes in nanopore surface area distribution are of similar characteristics. The percentage of nanopores larger than 5 nm largely decreases, while in the nanopore size range of 2–5 nm a relatively high plateau is observed. The peak value is only slightly lower than that of the uncompressed sample, while the location of the peak shifts toward the lower end by about 3 nm. Note that the overall specific nanopore surface area changes by only 2%, that is, existing nanopore surface does not vanish.

During the high-pressure loading, the nanopore structure is compressed by 0.5 cm^3/g. At the peak pressure, the nanopore space should be nearly entirely compressed. After unloading, the gas absorption analysis shows that there is a large residual nanopore volume of 0.34 cm^3/g, i.e., the nanoporous structure is partly recovered as the external load is fully removed, which fits with the observation that the slope of unloading curve rapidly decreases in the low-pressure stage. The recovered nanopores do not carry load at the second loading, and thus they must be formed by damaged walls. The weight density of the initial material is 742 mg/cm^3. Since it contains 0.54 cm^3/g of nanoporous space, the effective density of the network material is 1.6 g/cm^3. The weight density of the high-pressure compressed material is 1128 mg/cm^3, and therefore the effective density of network is 1.7 g/cm^3, close to the initial value, as it should be.

The collapse of nanopores provides a mechanism for plastic deformation. Usually, in a ceramic material, elastic deformation is dominated by atomic bonding, and plastic deformation is governed by behaviors of dislocations or atomic clusters, both of which are of characteristic lengths around 1 nm.[28] Since ordinary plastic-deformation mechanisms are inactive at room temperature,[29] when being compressed the pressure and the strain in a solid silica would increase linearly and, once the critical pressure is reached, cleavage fracture would occur. With the large volume fraction of nanopores, the silica gel behaves as a ductile material. Even though the network is brittle, due to the change of nanoporous structure, which is of a length scale comparable with that of a dislocation or an atomic cluster, the overall deformability is largely improved. Figure 5 depicts two possible collapse modes of a nanopore. In mode "a," the nanopore walls parallel to the external loading buckle. According to the classic linear elastic beam theory,[30] the buckling stress can be assessed as $\sigma_1 = \alpha E \rho / \rho_0$, where $\alpha \approx 0.05$ is a system parameter, E is the modulus of elasticity, ρ is the weight density of nanoporous phase, and ρ_0 is the weight density of network. For the silica gel investigated in the current study, as discussed above, $\rho = 0.74$ g/cm^3 and $\rho_0 = 1.6$ g/cm^3. If E is taken as 20 GPa,[31] the value of σ_1 is about 500 MPa, close to the measurement result. In mode "b," the reduction in nanoporous structure is caused by the bending and associated failure of nanopore walls normal to the external loading, for which the critical stress can be estimated as $\sigma_2 = \bar{\alpha} Y (\rho/\rho_0)^{3/2}$,[30] where $\bar{\alpha} \approx 0.3$ is a system parameter and Y is the strength of network material, which is 1–2 GPa for silica.[31] Thus, σ_2 is around 100–200 MPa, much smaller than the measured pressure of the compression plateau. It can be seen that the change in nanoporous structure should be dominated by mode "a." Although mode "b" requires a lower stress, it is suppressed, probably due to the irregular configuration and the contoured paths of nanopores, the interconnected nanopore structure, etc.

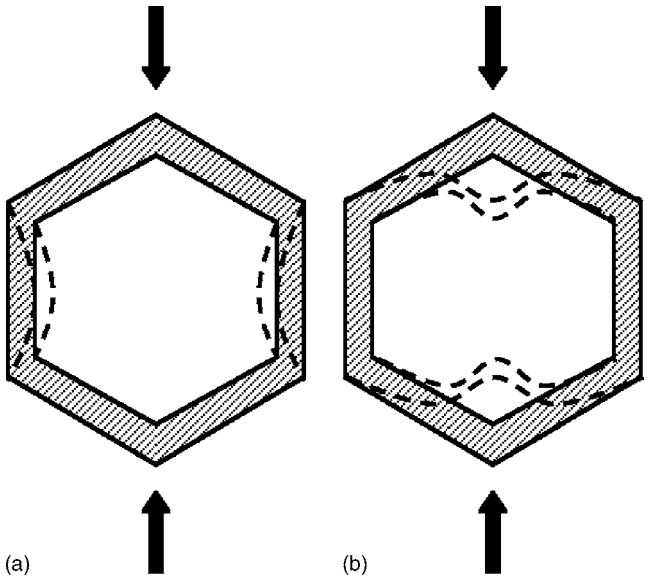

FIG. 5. Schematic of possible failure modes of nanopore walls: (a) parallel and (b) normal to the external loading. The arrows indicate the direction of external loading.

The energy absorption capacity related to the nanopore collapse can be calculated as the area enclosed by the loading-unloading cycle, which is nearly 300 J/g. This value is higher by orders of magnitude than that of many conventional protection and damping materials, such as reinforced polymers and shape memory alloys.[32] It is also much higher than that of NMF liquids. For instance, if the nanoporous silica gel is surface treated and immersed in an aqueous solution of electrolyte, the energy absorption efficiency is 10–30 J/g.[33–36] Even if liquids of larger surface tensions are utilized, the maximum energy absorption efficiency is only about 100 J/g.[37,38] The high energy absorption performance of the nanoporous silica gel should be attributed to the small nanopore size, the relatively large porosity, as well as the high network strength.

IV. CONCLUDING REMARKS

The behaviors of a nanoporous silica gel under compressive loading are investigated. When the pressure is relatively low, the specific volume change is caused by the packing of silica particles. When the pressure is relatively high, the

nanoporous structure collapses, leading to an energy absorption efficiency higher by orders of magnitude than that of many protection and damping materials. The material deforms in a ductile manner. The plastic deformation is dominated by the buckling of nanopore walls parallel to the external loading, which is of a similar characteristic length to that of dislocations and atomic clusters. Classic poromechanics theory works relatively well for compression stress analysis. After the high-pressure test, while the nanopore volume is considerably decreased, the change in nanopore surface area is negligible.

ACKNOWLEDGMENTS

This study was supported by the Army Research Office under Grant No. W911NF-05-1-0288.

[1]S. Abdennadher and H. Zhao, Int. J. Veh. Des. **37**, 156 (2005).
[2]L. J. Gibson and M. F. Ashby, *Cellular Solids: Structure and Properties* (Cambridge University Press, Cambridge, UK, 1999).
[3]P. A. Du Bois, S. Killing, M. Koesters, and T. Frank, Int. J. Impact Eng. **32**, 725 (2006).
[4]J. Banhart, Prog. Mater. Sci. **46**, 559 (2001).
[5]E. Andrews, W. Sanders, and L. J. Gibson, Mater. Sci. Eng., A **270**, 113 (1999).
[6]W. J. Stronge, *Impact Mechanics* (Cambridge University Press, Cambridge, UK, 2004).
[7]C. J. Benning, *Plastic Foams* (Wiley, New York, 1970).
[8]A. H. Landrock, *Handbook of Plastic Foams* (Noyes, Park Ridge, NJ, 1995).
[9]D. Exerowa and P. M. Kruglyakov, *Foam and Foam Films* (Elsevier Science, Amsterdam, 1997).
[10]T. W. Clyne and F. Simancik, *Metal Matrix Composites and Metallic Foams* (Wiley-VCH, New York, 2000).
[11]H. J. Pain, *The Physics of Vibrations and Waves* (Wiley, New York, 2005).
[12]C. C. Chamis, J. Reinf. Plast. Compos. **26**, 987 (2007).
[13]Y. Zhu, Y. Hu, and F. Miura, Proceedings of The Fifth International Conference on Nonlinear Mechanics, Shanghai, China, 10–14 June 2007.
[14]A. Zukal, Chem. Listy **101**, 208 (2007).
[15]U. Ciesla and F. Schuth, Microporous Mesoporous Mater. **27**, 131 (1999).
[16]J. Biener, A. M. Hodge, A. V. Hamza, L. M. Hsiung, and J. H. Satcher, J. Appl. Phys. **97**, 024301 (2005).
[17]F. Ebrahimi, Q. Zhai, and D. Kong, Scr. Mater. **39**, 315 (1998).
[18]G. H. Lee, C. K. Rhee, M. K. Lee, W. W. Kim, and V. V. Ivanov, Mater. Sci. Eng., A **375-377**, 604 (2004).
[19]M. C. Johnson, J. L. Wang, Z. J. Li, C. A. Lew, and Y. S. Yan, Mater. Sci. Eng., A **456**, 58 (2007).
[20]E. P. Guyer, M. Patz, and R. H. Dauskardt, J. Mater. Res. **21**, 882 (2006).
[21]F. B. Surani, X. Kong, and Y. Qiao, Appl. Phys. Lett. **87**, 251906 (2005).
[22]F. B. Surani, X. Kong, D. B. Panchal, and Y. Qiao, Appl. Phys. Lett. **87**, 163111 (2005).
[23]X. Kong and Y. Qiao, Appl. Phys. Lett. **86**, 151919 (2005).
[24]X. Kong, F. B. Surani, and Y. Qiao, J. Mater. Res. **20**, 1042 (2005).
[25]X. Kong and Y. Qiao, Philos. Mag. Lett. **85**, 331 (2005).
[26]X. Chen, F. B. Surani, X. Kong, V. K. Punyamurtula, and Y. Qiao, Appl. Phys. Lett. **89**, 241918 (2006).
[27]S. Ulku, D. Balkose, and H. Baltacboglu, Colloid Polym. Sci. **271**, 709 (1993).
[28]T. J. Chuang, *Nanomechanics of Materials and Structures* (Springer, New York, 2006).
[29]F. A. McClintock and A. S. Argon, *Mechanical Behaviors of Materials* (Addison-Wesley, Reading, MA, 1966).
[30]M. F. Ashby and D. R. H. Jones, *Engineering Materials II* (Butterworth Heinemann, London, 1998).
[31]N. P. Bansal and R. H. Doremus, *Handbook of Glass Properties* (Academic, New York, 1986).
[32]G. Lu and T. Yu, *Energy Absorption of Structures and Materials* (CRC, Boca Raton, FL, 2003).
[33]A. Han and Y. Qiao, J. Am. Chem. Soc. **128**, 10348 (2006).
[34]Y. Qiao, V. K. Punyamurtula, A. Han, X. Kong, and F. B. Surani, Appl. Phys. Lett. **89**, 251905 (2006).
[35]F. B. Surani, A. Han, and Y. Qiao, Appl. Phys. Lett. **89**, 093108 (2006).
[36]F. B. Surani and Y. Qiao, J. Appl. Phys. **100**, 034311 (2006).
[37]V. K. Punyamurtula and Y. Qiao, Mater. Res. Innovations **11**, 37 (2007).
[38]V. K. Punyamurtula, A. Han, and Y. Qiao, Adv. Eng. Mater. **9**, 209 (2007).